HIGH-CYCLE FATIGUE OF BETA TITANIUM ALLOYS

J. O. Peters*[+], G. Lütjering*, R. K. Nalla**, I. Altenberger**, R. O. Ritchie**

This study compares the high-cycle fatigue (HCF) properties of the high-strength β titanium alloys β–Cez and Ti-6246 (in two distinctly different $\alpha+\beta$ processed and β processed conditions) with the conventional $\alpha+\beta$ titanium alloy Ti-6Al-4V (in a $\alpha+\beta$ processed condition). The first part of the work addresses the superior fatigue-crack initiation resistance and smooth-bar HCF strength of β–Cez and Ti-6246 compared to Ti-6Al-4V. In the second part, the problem of foreign-object damage on jet engine fan blades is used as an engineering example of potential HCF applications for β titanium alloys.

INTRODUCTION

This paper compares the high-cycle fatigue (HCF) properties of the high-strength β titanium alloys β–Cez and Ti-6246 with the conventional $\alpha+\beta$ titanium alloy Ti-6Al-4V. It is motivated by an increasing interest in replacing $\alpha+\beta$ titanium alloys with β titanium for highly-stressed airframe and engine components. This comparative study includes two distinctly different $\alpha+\beta$ processed and β processed microstructures in β–Cez and Ti-6246, and a $\alpha+\beta$ processed microstructure in Ti-6Al-4V. In the first part, the smooth-bar stress-life (S-N) fatigue behavior of $\alpha+\beta$ and β titanium alloys was investigated, with specific emphasis on the underlying microstructural aspects of the superior high-cycle fatigue (HCF) strength of the β titanium alloys.

The latter part of the paper focuses on foreign-object damage (FOD), which has been identified as one of the prime causes of HCF failures in military aircraft engines (e.g., Cowles [1]). The objective here is to investigate the role of FOD in affecting the initiation and early growth of small surface fatigue cracks under HCF conditions in Ti-6246 alloy (in both microstructures), and to compare the results with previous data for Ti-6Al-4V. FOD was simulated using high-velocity impacts of steel shot on the flat surface of fatigue test specimens, as used in prior work by Peters et al. [2] on Ti-6Al-4V. This study indicated that FOD could severely reduce

*Technical University Hamburg-Harburg, Germany. **University of California, Berkeley, CA, USA.
[+]Contact author's address: TU Hamburg-Harburg, 21071 Hamburg, Germany. E-Mail: j.o.peters@tu-harburg.de

the fatigue strength due to several factors, including the stress concentration associated with the damage site, the formation of FOD-induced microcracks, impact induced plasticity and tensile residual stresses resulting from the impact. In this study, we attempt to extend the Kitagawa-Takahashi approach, which was proposed in [2] to account for the effect of FOD on HCF failures in Ti-6Al-4V, to the higher-strength β titanium alloys.

MATERIALS AND EXPERIMENTAL PROCEDURES

The β titanium alloys, β–Cez (wt.%-Ti-5.0Al-1.9Sn-4.5Zr-3.9Mo-2.2Cr-1.1Fe-0.1O, produced by CEZUS, France, and supplied by Boehler Schmiedetechnik GmbH, Austria) and Ti-6246 (wt.%-Ti-5.8Al-2Sn-4Zr-6Mo-0.1O, produced by Timet, USA, and supplied by Otto Fuchs Metallwerke, Germany), were $\alpha+\beta$ or β processed to produce, respectively, fine-grained bi-modal and larger pancake-shaped grained microstructures. The Ti-6Al-4V alloy (wt.%-Ti-6.3Al-4.2V-0.2Fe-0.2O) was processed to a $\alpha+\beta$ processed fine-grained equiaxed microstructure and supplied by the U.S. Air Force HCF program (Eylon [3]). Processing details are given below and are listed in Table 1.

For the fine-grained bi-modal microstructures of the β–Cez and Ti-6246 alloys shown in Figs. 1a and 1d, respectively, the as-received $\alpha+\beta$ processed bar stock material was initially cross rolled (at TUHH) in the $\alpha+\beta$ phase field followed by air cooling. Recrystallization at relatively high temperatures in the $\alpha+\beta$ phase field resulted in a low volume fraction of the primary α phase and a β grain size of ~40 μm. During subsequent controlled cooling, continuous α layers formed at β grain boundaries and α plates precipitated within β grains. To coarsen these α plates and to adjust the volume fraction of α plates, specimen blanks were annealed below the recrystallization temperature (Table 1), followed by controlled cooling. Finally, blanks of the $\alpha+\beta$ processed material were aged to precipitate small incoherent secondary α platelets between coarse α plates.

For the β–Cez and Ti-6246 microstructures with large pancake-shaped β grains, two different β processing procedures were used at Boehler Schmiedetechnik (for β–Cez) and at Fuchs Metallwerke (for Ti-6246) [4,5]. For the β–Cez alloy, the bar stock material was initially heated into the β phase field, which resulted in a β grain size of ~400 μm, taken out of the furnace and subsequently forged through the β transus (890°C) into a slab. The final temperature was ~850°C. Using a deformation degree of φ = 0.9, the relatively large equiaxed β grains were flattened into pancake-shaped β grains (1000 x 650 x 260 μm), as shown in Fig. 1b. During air cooling after the forging process, a more or less continuous α layer formed at β grain boundaries and α plates precipitated within the β grains. The subsequent heat treatments were identical to the $\alpha+\beta$ process in order to achieve the same strength level, namely annealing to coarsen the large α plates and to control their volume fraction, followed by aging step to precipitate small secondary α platelets. The microstructure of the β processed microstructure in the β–Cez alloy after final heat treatment is shown in Fig. 1c. For the Ti-6246 alloy, bar material was also heated into the β field, which resulted in a β grain size of ~750 μm, and then deformed in

the β field at 965°C (β-transus 945°C), followed by fast cooling to inhibit the recrystallization of deformed β grains (1200 x 1200 x 200 μm). Again, the final annealing and aging treatment in the $\alpha+\beta$ phase field was identical to that used for the $\alpha+\beta$ processed bi-modal Ti-6246 alloy to achieve the same strength level. Fig. 1e shows the coarse α plates within the pancake-shaped β grains and the more or less continuous α layer at the β grain boundaries of the β processed Ti-6246 after final heat treatment.

The fine-grained Ti-6Al-4V material, shown in Fig. 1f, was forged in one stroke in the $\alpha+\beta$ phase field (940°C) to a plate size of 400 x 150 x 20 mm. Subsequently, the forged plates were recrystallized in the $\alpha+\beta$ phase field (at 930°C) to adjust the volume fraction of primary α phase to ~60% (diameter ~20 μm). During subsequent fan air cooling, α lamellae precipitated within the β grains. Finally, the plate material was stress relieved for 2 hr at 705°C. This fine-grained equiaxed microstructure has been termed "solution treated and overaged" (STOA).

The tensile properties of the β–Cez, Ti-6246 and Ti-6Al-4V alloys are listed in Table 2. The pancake structures were tested in the L-direction. Further details on the tensile and fatigue testing are given in [2,4], and on the FOD simulation in [2].

SMOOTH-BAR FATIGUE PROPERTIES

Smooth-bar stress-life (S-N) fatigue data (R = -1) for both $\alpha+\beta$ and β processed β–Cez and Ti-6246 alloys, are compared with results on Ti-6Al-4V in Fig. 2. All tests were performed on electrolytically-polished hourglass-shaped specimens.

It can be seen that the β–Cez and Ti-6246 conditions show a much higher 10^7-cycle HCF endurance strength (σ_{HCF} = 575-625 MPa) compared to Ti-6Al-4V (σ_{HCF} = 375 MPa). The superior HCF strength of the β alloys is primarily due to their higher yield strength. HCF strength is primarily controlled by resistance to fatigue-crack nucleation, i.e., to first dislocation slip, although microstructure and texture can play an important role. Crack-initiation sites in the $\alpha+\beta$ processed and β processed β alloy microstructures are shown for β–Cez in Fig. 3 in comparison to Ti-6Al-4V. In the Ti-6246 and β–Cez alloys, fatigue cracks preferentially initiated along the α/β interfaces of coarse α plates within the β grains, as shown in Fig. 3a ($\alpha+\beta$ processed) and Fig. 3b (β processed). These interfaces can be identified as microstructurally-weak crack-initiation sites because of the incompatibility of strains at the interface. (A thin volume of β matrix adjacent to the α plates is plastically deformed by a slip-band mechanism, as there are no hindering secondary α platelets within this thin volume and the coarse α plates remain undeformed). The higher HCF strength of the $\alpha+\beta$ processed structure can be attributed to the smaller β grain size (which effectively limits the maximum length of the α plates), in comparison with the larger dimensions of the β grains in the β processed structures (even in the thickness direction). The continuous α-layer at β grain boundaries, which is the weakest crack-nucleation site in the β alloys, apparently was very difficult to activate because the pancake structure was tested in L-direction and in the bi-modal structure the β grain-boundary length is smaller than the α plate

length. In the $\alpha+\beta$ processed Ti-6Al-4V microstructure, fatigue cracks tend to initiate within the primary α phase along planar slip bands (Fig. 3c). Whereas the lower HCF strength of the Ti-6Al-4V alloy may be primarily controlled by the lower yield strength ($\sigma_{0.2}$), the low $\sigma_{HCF}/\sigma_{0.2}$ ratio of ~0.41 (Table 2) can be explained by the high volume fraction of interconnecting primary α grains, which show strong crystallographic texture and which increase the effective maximum slip length from a single α grain diameter to several grain diameters.

To investigate the role of mean stress in Ti-6246 (as an example of β Ti alloys), smooth-bar *S-N* fatigue tests were performed at higher load ratios of $R = 0.1$ and 0.5 and compared to results for the $\alpha+\beta$ Ti-6Al-4V alloy. Resulting *S-N* curves for these alloy conditions are shown in Fig. 4, and indicate that increasing the load ratio, and hence the mean stress, results in a higher limiting value of applied maximum stress necessary to cause HCF failure; the corresponding limiting stress amplitude is decreased. Generally, the Ti-6246 microstructures show superior HCF strength at higher load ratios compared to the $\alpha+\beta$ processed Ti-6Al-4V alloy. Whereas at load ratios of $R = -1$ and 0.1, both Ti-6246 microstructures show effectively the same HCF strength, at $R = 0.5$ the β processed condition clearly has a much higher HCF strength than the $\alpha+\beta$ processed condition. Typical crack-initiation sites at $R = 0.5$ are illustrated in Fig. 5 for both Ti-6246 microstructures. Of particular note is the observation that the preferred sites for crack initiation changed from the interface of the coarse α plates at low *R*-ratios to the interface of the α layers at β grain boundaries at $R = 0.5$. Apparently, the higher maximum stress at $R = 0.5$ can cause the coarse α plates to plastically deform, which reduces the incompatibility strains at the α plate interface. Indeed, this explanation should also apply for the $\alpha+\beta$ processed bi-modal condition. The lower HCF strength at $R = 0.5$ of the bi-modal structure, compared to that of the β processed structure (Fig. 4), indicates that the next crack-nucleation site which would then be activated is much weaker in the former condition. Because of the fineness of the bi-modal structure, however, it is difficult to identify an alternative crack-nucleation site unambiguously, and further work is necessary before definitive conclusions can be made.

EFFECT OF FOD ON FATIGUE PROPERTIES

To investigate FOD-induced HCF failures in β titanium alloys and to compare with previous results [2] for Ti-6Al-4V, FOD was simulated using high velocity (200 and 300 m/s) impacts of 3.2 mm diameter steel spheres on the flat surface of fatigue test specimens. It was found that both microstructures in Ti-6246 showed similar states of damage. A typical impact damage site after a 300 m/s impact for the $\alpha+\beta$ microstructure in Ti-6246 is shown in Fig. 6. Although impact craters in Ti-6246 were ~5% smaller in size than in Ti-6Al-4V (due to higher strength of Ti-6246), once again similar states of damage were observed. Specifically, impact velocities greater than 200 m/s caused circumferentially-oriented intense shear bands to form, which emanated from the surface of the impact crater; in addition, a pronounced plastic pile-up of material occurred at the crater rim, resulting in the formation of

multiple notches and microcracks. These small cracks, which were ~5 to 70 μm in surface length, were found to act as the preferred initiation sites for fatigue cracking during subsequent cycling. Consequently, the smooth-bar *S-N* fatigue life is significantly reduced by prior high-velocity impact damage (Fig. 7). Although the presence of the FOD-induced microcracks represents the primary cause of the reduced fatigue resistance, the stress concentration factor associated with the indent (k_t ~ 1.25), the deformed microstructure beneath the indent and the tensile residual stresses resulting from the impact are contributing factors.

Although only seven Ti-6246 specimens were tested, two groups of failures could be identified (Fig. 7). As noted, for 300 m/s impacts, FOD caused the formation of microcracks at the crater rim, which served as the initiation sites for subsequent fatigue cracking (the surface crack lengths are indicated in Fig. 7). Fatigue-crack initiation after slower 200 m/s impacts occurred at locations remote for the indent crater (Fig. 8), specifically in regions where numerical computations [6] have confirmed the existence of relatively high (~350 MPa) tensile residual stresses.* These tensile stresses act to elevate the *local* load ratio when simply superimposed on the applied fatigue loading. For applied cyclic maximum stresses of 500 MPa, superimposing a tensile residual stress of ~350 MPa causes an increase in the local load ratio from 0.1 to about 0.5, assuming no relaxation; the corresponding increase in the maximum stress is indicated by arrows in Fig. 7. From these *S-N* results, it is clear that the simple superposition of the applied and initial tensile residual stresses contributes significantly to the reduction in fatigue life from FOD through a local elevation in the *R*-ratio.

For 300 m/s impacts, all Ti-6246 and Ti-6Al-4V microstructures studied showed comparable fatigue strengths following simulated FOD (Fig. 7), presumably because similar-sized impact-induced microcracks were formed and served as initiation sites for fatigue cracking. In contrast, for 200 m/s impacts where microcracks were not formed, the Ti-6246 alloy exhibited a higher fatigue strength than the Ti-6Al-4V material investigated; this relates to its superior intrinsic resistance to fatigue-crack initiation, as evidenced by its higher smooth-bar HCF strength (Fig. 4).

Based on recent work on Ti-6Al-4V [2,7] where a modified Kitagawa-Takahashi approach [8] was proposed for the characterization of a threshold envelope for FOD-induced HCF failures, Fig. 9 shows a similar characterization (at R = 0.1) for both microstructures in Ti-6246, with results compared to α+β processed Ti-6Al-4V. Failure points are corrected for the stress concentration from the indent and can be seen to be bounded by threshold envelopes defined at small crack sizes in terms of smooth-bar fatigue limit (for Ti-6246: $\Delta\sigma_{HCF}$ = 630 MPa; for Ti-6Al-4V: $\Delta\sigma_{HCF}$ = 450 MPa), and at large "continuum-sized" crack sizes in terms of the "worst-

* This peak tensile residual stress in Ti-6246 was higher than the corresponding value of 300 MPa computed for Ti-6Al-4V, the latter value being experimentally verified using synchronous X-ray diffraction measurements [7].

case" fatigue-crack growth threshold.** Small crack threshold results would be preferred here to define these threshold envelopes, e.g., in the Ti-6Al-4V material investigated, ΔK_{TH} values as low as 1.0-1.5 MPa$\sqrt{m}$ have been measured at 10^{-10} m/cycle [9], but such data in general are difficult to collect experimentally. However, the worst-case threshold concept [10] provides a reasonable and sound engineering alternative.

CONCLUSIONS

Based on a study of high-cycle fatigue in high-strength β titanium alloys β–Cez and Ti-6246 (in both $\alpha+\beta$ and β processed conditions), as compared to conventional $\alpha+\beta$ titanium alloy Ti-6Al-4V (in an $\alpha+\beta$ processed condition), the following conclusions can be drawn:

1. The smooth-bar high-cycle fatigue strength of the β–Cez and Ti-6246 alloys at R = -1 (σ_{HCF} = 575-625 MPa) was found to be superior to that of the $\alpha+\beta$ processed Ti-6Al-4V material (σ_{HCF} = 375 MPa), primarily because of the higher strength of the β titanium microstructures. The Ti-6246 microstructures also displayed higher HCF strengths at R = 0.1 and 0.5. This is reflective of an increased resistance to fatigue crack initiation in Ti-6246.
2. For β titanium alloys, principally at a low R-ratio of -1, fine-grained $\alpha+\beta$ processed bi-modal microstructures were found to exhibit higher smooth-bar HCF strengths than coarse-grained β processed microstructures with pancake-shaped grains (tested in L-direction). However, this ranking was reversed at higher load ratios (R = 0.5), where the β processed microstructure showed the superior HCF properties.
3. Both the investigated microstructures in Ti-6246 showed similar states of damage and similar reductions in HCF strength following simulated FOD. Although impact sites were ~5% smaller than in Ti-6Al-4V (due to the higher strength of Ti-6246), the nature of the damage and the resulting effect on fatigue strengths were similar in both alloys.
4. The principal effect of FOD in reducing the HCF strength was to introduce preferential sites for the premature initiation of fatigue cracks. However, other factors include the interplay of (i) the stress concentration due to the indentation, (ii) the creation of microcracks at the damage site (for higher impact velocities), (iii) the deformed microstructure beneath the indent, and (iv) the presence of localized tensile residual stresses around the impact site.
5. For both Ti-6246 and Ti-6Al-4V alloys, two groups of failures could be identified. At 300 m/s impact velocities, where FOD induced microcracks were formed, fatigue cracks initiated from these microcracks at the crater rim.

** "Worst-case" ΔK_{TH} values can be considered as lower-bound large-crack thresholds; they are measured with large through-thickness cracks on compact-tension specimens at load ratios approaching unity, i.e., as $K_{max} \rightarrow K_{Ic}$, in order to minimize any role of crack closure [10]. Values are listed in Table 2.

However, for 200 m/s impacts, fatigue cracks were found to initiate away from the indent crater, in regions of relatively high tensile residual stresses (~300-350 MPa).

6. Threshold conditions for FOD-induced HCF failures in both Ti-6246 and Ti-6Al-4V titanium alloys were proposed based on a modified Kitagawa-Takahashi diagram, where the limiting conditions are described in terms of the smooth-bar fatigue limit at small crack sizes and the "worst-case" (large-crack) fatigue-crack growth threshold.
7. For high-stress HCF and FOD-critical applications, such as fan and compressor blades, where critical crack sizes can be as small as 500 μm or less, the use of high-strength β titanium alloys, such as Ti-6246, appears to be preferable choice to the currently used Ti-6Al-4V alloys. This is because of their superior fatigue-crack initiation resistance (in the form of a higher smooth-bar HCF strength) and only marginally lower fatigue-crack propagation resistance (in terms of a slightly lower "worst-case" large-crack threshold).

ACKNOWLEDGEMENTS

Work on Ti-6Al-4V was supported by the Air Force Office of Science and Research, Grant No. F49620-96-1-0478, under the Multidisciplinary University Research Initiative on "High Cycle Fatigue" to the University of California, Berkeley. Special thanks are due to Prof. J. W. Hutchinson, Dr. X. Chen and Dr. B. L. Boyce for helpful discussions and providing us with their results.

REFERENCES

(1) Cowles, B.A., *Int. J. Fract.*, Vol. 80, 1996, pp. 147-63.

(2) Peters, J.O., Ritchie, R.O., *Eng. Fract. Mech.*, Vol. 67, 2000, pp. 193-207.

(3) Eylon, D., Summary of the available information on the processing of the Ti-6Al-4V HCF/LCF program plates., University of Dayton Report, Dayton, OH, 1998.

(4) Peters, J.O., Lütjering, G., *Metall. Mater. Trans. A*, Vol. 32A, 2001, pp. 2805-15.

(5) Sauer, C., Lütjering, G., *Mat. Process. Tech.*, Vol. 117, 2001, pp. 311-17.

(6) Chen, X., Hutchinson, J.W., unpublished research, Harvard University, 2001.

(7) Peters, J.O., Boyce, B.L., Chen, X., McNaney, J.M., Hutchinson, J.W., Ritchie, R.O., *Eng. Fract. Mech.*, Vol. 69, 2002, in press.

(8) Kitagawa, H., Takahashi, S., *Proc. 2nd Int. Conf. on Mechanical Behavior of Materials,* Metals Park, OH; ASM, 1976, pp. 627-31.

(9) Hines, J.A., Peters, J.O., Lütjering, G., *Titanium'99, Science and Technology, Proc. 9th World Congress on Titanium*. Edited by Gorynin, I., Ushkov, S.S., Central Research Institute of Structural Materials (CRISM) "Prometey", St. Petersburg, Russia, 2000, pp. 433-40

(10) Boyce, B.L., Ritchie, R.O., *Eng. Fract. Mech.*, Vol. 68, 2001, pp. 129-47.

TABLE 1 Processing and heat treatment of the titanium alloys studied

Alloy	Microstructure (Processing)	Deformation	Heat Treatment	Cooling Rate (°C/min)
β-Cez	Bi-modal $\alpha+\beta$ processed	850°C, φ = -1.3	1 hr 870°C, 1 hr 820°C, 8 hr 580°C	100
β-Cez	Pancake $\beta \rightarrow \alpha+\beta$ deformed	920°C→850°C, φ = -0.7	1 hr 820°C, 8 hr 580°C	100
Ti-6246	Bi-modal $\alpha+\beta$ processed	905°C, φ = -1.0	1 hr 935°C, 1 hr 910°C, 8 hr 595°C	50
Ti-6246	Pancake β deformed	965°C, φ = -1.0	1 hr 915°C, 8 hr 595°C	50
Ti-6Al-4V	Equiaxed $\alpha+\beta$ processed	940°C, φ = -1.2	1 hr 930°C, 2 hr 705°C	100

TABLE 2 Tensile properties, fatigue ratios, and "worst-case" fatigue-crack growth thresholds

Alloy	Condition	$\sigma_{0.2}$ (MPa)	*UTS* (MPa)	*RA* (%)	$\sigma_{HCF}/\sigma_{0.2}$ (R = -1)	worst-case ΔK_{TH} (MPa$\sqrt{m}$)
β–Cez	$\alpha+\beta$ proc.	1200	1275	34	0.52	-
β–Cez	β proc.	1190	1275	16	0.48	-
Ti-6246	$\alpha+\beta$ proc.	1050	1155	42	0.55	1.5 (R = 0.94)
Ti-6246	β proc.	1055	1170	15	0.55	1.5 (R = 0.94)
Ti-6Al-4V	$\alpha+\beta$ proc.	915	965	45	0.41	1.9 (R = 0.95)

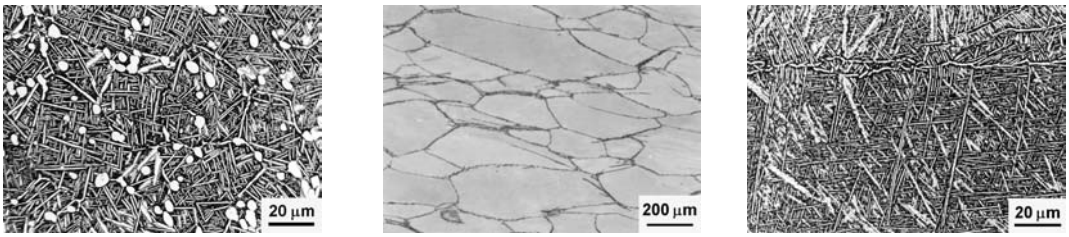

a) β–Cez, $\alpha+\beta$ processed b) β–Cez, β proc. pancake grains c) β–Cez, β processed

d) Ti-6246, $\alpha+\beta$ processed e) Ti-6246, β processed f) Ti-6Al-4V, $\alpha+\beta$ processed

FIGURE 1 Microstructures of titanium alloys studied.

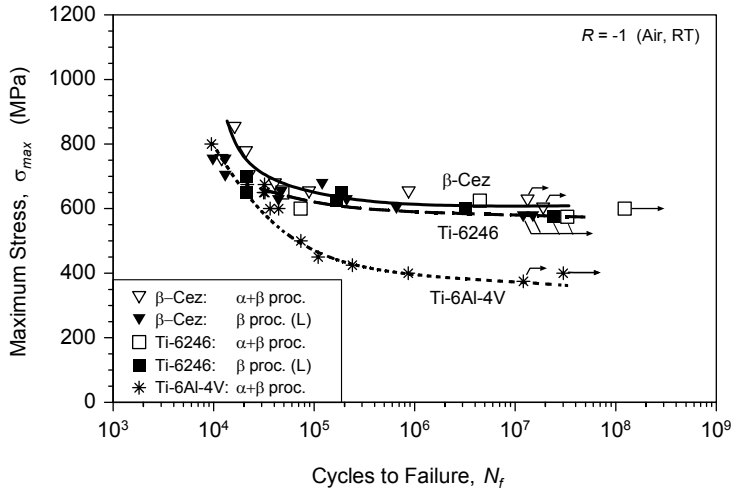

FIGURE 2 *S-N* curves of the β-Cez, Ti-6246, and Ti-6Al-4V microstructures studied.

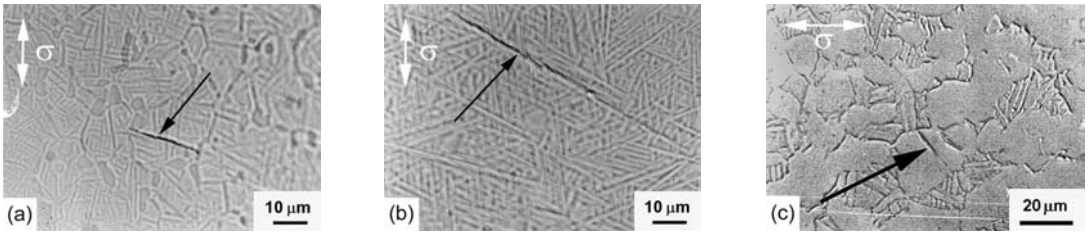

FIGURE 3 Fatigue crack initiation sites (R = -1) for a) β-Cez ($\alpha+\beta$ processed), b) β-Cez (β processed), and c) Ti-6Al-4V ($\alpha+\beta$ processed) alloys.

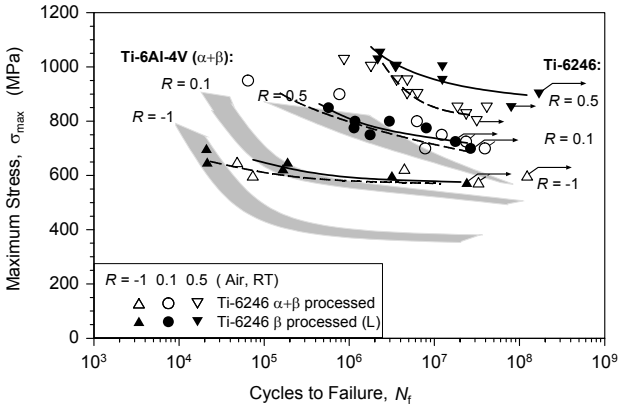

FIGURE 4 Smooth-bar *S-N* data of Ti-6246 microstructures at R = -1, 0.1, and 0.5, as compared to Ti-6Al-4V.

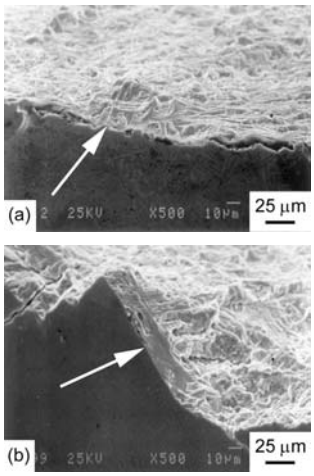

FIGURE 5 Fatigue crack initiation sites in Ti-6246 in the a) $\alpha+\beta$, b) β processed states.

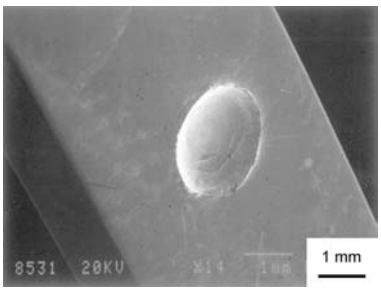

FIGURE 6 300 m/s FOD impact in Ti-6246, $\alpha+\beta$ processed.

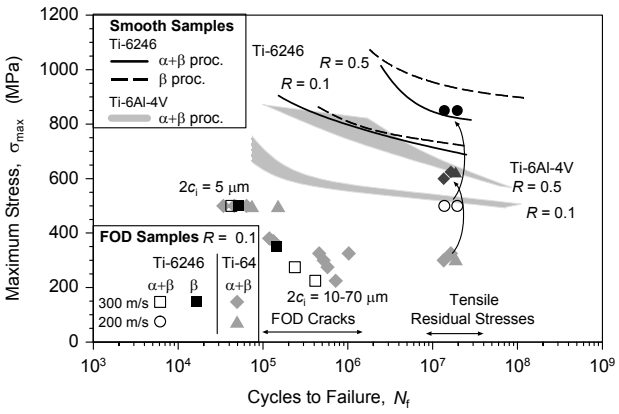

FIGURE 7 *S-N* data of FOD impacted and smooth-bar specimens for all alloys.

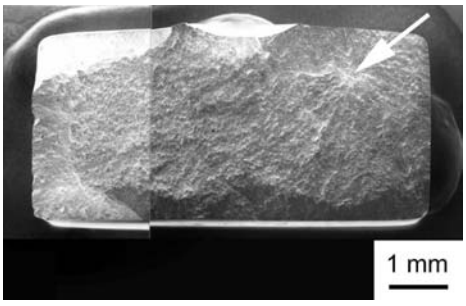

FIGURE 8 Residual stress-induced fatigue failure of a FODed sample.

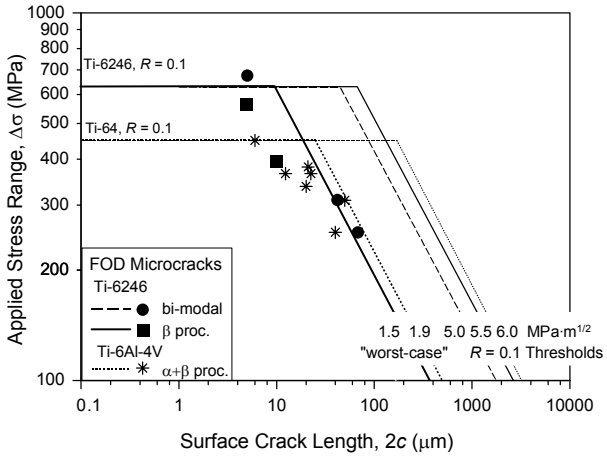

FIGURE 9 Kitagawa-Takahashi diagram for FOD-affected HCF thresholds.